# SPIRAL ELECTROSPUN PLA/GO POROUS NANOFIBER MEMBRANES
## Tuning Properties via Graphene Oxide Incorporation

by

***Jianming WANG[a], Ya CHEN[b], Lei ZHAO[a,c,d*], Danni YU[c], Li WEI[a], Kuikui ZONG[e], Chunxia WANG[f], Chunqin MA[g], and Qihu BU[g]***

[a] Textile and Clothing College, Yancheng Polytechnic College, Yancheng, China
[b] College of Materials Science and Engineering, Yancheng Institute of Technology, Yancheng, China
[c] College of Textile and Clothing Engineering, Soochow University, Suzhou, China
[d] Institute of Flexible Functional Materials, Yancheng Institute of Technology, Yancheng, China
[d] Suzhou Jingfei Textile Technology Co., Ltd., Suzhou, China
[f] College of Textile and Clothing, Yancheng Institute of Technology, Yancheng, China
[g] Jiangsu Yueda Textile Group Co., Ltd., Yancheng, China

Original scientific paper
https://doi.org/10.2298/TSCI2602217W

*This study focuses on the fabrication of polylactic acid/graphene oxide (PLA/GO) porous nanofiber membranes using spiral electrospinning technology. With PLA as the solute and nanographene oxide as the additive, the optimal process parameters for preparing pure PLA porous nanofibers were first determined through orthogonal experiments. Then, PLA/GO composite nanofibers with different GO contents (0.1 wt.%, 0.2 wt.%, 0.5 wt.%, 1.0 wt.%) were prepared. A series of characterization techniques, including Fourier-transform infrared spectroscopy, X-ray diffraction, pore size distribution analysis, mechanical testing, and contact angle measurement, were employed to comprehensively analyze the effects of GO addition on the structure and properties of the nanofiber membranes. The results reveal that the addition of GO significantly enhances the mechanical properties of the PLA/GO composite fiber membranes, with notable improvements in fiber fracture strength and elongation at break. Meanwhile, the addition of GO has no significant impact on the wetting performance and crystal structures of the fiber membranes. As the content of oxidized graphite increases, the average pore size decreases and the total number of pores increases These findings lay a solid foundation for further exploring the adsorption properties of PLA/GO porous nanofibers and expand their potential applications in various fields.*

Key words: *electrospinning, porous nanofiber membrane, PLA, GO, mechanical properties, wetting performance, pore size*

## Introduction

Porous structural materials, *e.g.*, porous concretes [1, 2], porous coals [3, 4], and porous nanofibers [5], have become a focal point in materials science research, boasting a plethora of applications across diverse domains, including adsorption, separation, catalysis, and tissue engineering. The development of methods to fabricate these materials has been a long

* Corresponding author, e-mail: zhaolei7365@163.com

standing pursuit. The sol-gel method, a widely employed technique, capitalizes on the hydrolysis and condensation of metal alkoxides or organic precursors to create porous architectures [6-8]. Hydrothermal synthesis, another popular approach, facilitates the growth of porous materials under high temperature and high pressure aqueous conditions, enabling meticulous control over crystal growth and pore formation [9-11]. Researchers have also explored alternative methods such as the precipitation method, template method, and phase inversion method [12-14]. However, the synthesis of porous nanofibers remains a challenge for these traditional techniques, mainly due to complex reaction conditions, difficulties in precisely tailoring nanofiber morphology, and high production costs.

Electrospinning [5] has emerged as a powerful and versatile technique for fabricating porous nanofibers. It offers distinct advantages, including simplicity of operation, the ability to produce nanofibers with a high surface-to-volume ratio, and flexibility in material selection. The formation of pores in electrospun nanofibers can be achieved through two primary mechanisms: liquid-phase separation induced pore formation and solid-phase separation pore forming method.

Liquid-phase separation induced pore formation in electrospinning is a process where a spinning solution containing volatile solvents is ejected from a syringe into an electric field. In this environment, the solvents evaporate rapidly, leading to the formation of porous structures both within and on the surface of the fibers. Bognitzki *et al.* [10] were the first to prepare a spinning solution with PLA, polycarbonate, and polyvinylcarbazole as solutes and dichloromethane as the solvent. Under an applied voltage, they successfully fabricated uniformly distributed, disordered porous nanofibers. Subsequently, Zhu *et al.* [11] exploited the polarization of the electric dipole component along the main carbon chain of PLA in the orientation direction to prepare ordered porous PLA nanofibers. Their work further delved into potential applications in strain sensing and energy harvesting.

The solid-phase separation pore formation method involves incorporating multiple polymers or inorganic salts into the spinning solution. Subsequently, the solid-phase components are removed through post-treatment processes such as washing, heat treatment, or UV irradiation. This leaves behind a multitude of pores in the locations previously occupied by the solid phase, thereby creating a porous structure. Generally, the solid-phase separation pore formation method is a multi-step approach. While it is more intricate than some other methods, it offers precise control over the size and shape of the pores.

Li *et al.* [12] utilized $LaFeO_3$ and PVP as spinning solvents and employed heat treatment to prepare pure porous $LaFeO_3$ nanofibers. These nanofibers possess outstanding structural characteristics and a high specific surface area, which endows them with promising application prospects in the realm of photocatalytic adsorption. Chen *et al.* [13] fabricated porous polypropylene fibers by using PMMA as a pore forming agent and PAN as a solute. They further modified these fibers to enhance their ability to adsorb heavy metal chromium. Lyoo *et al.* [14] prepared nanofiber membranes from a mixture of PVCi/PHBV/$CHCl_3$ through UV irradiation. Subsequently, UV treatment was applied to trigger a cross-linking reaction in PVCi, rendering it insoluble. The PHBV was then extracted and removed using $CHCl_3$, ultimately resulting in the formation of a porous fiber structure. Li *et al.* [15] successfully synthesized PLA nanoporous fiber membranes by integrating the thermal nonsolvent induced phase separation technique with electrospinning in a PLA/DCM single solvent system. Their findings indicated that the nanoporous membranes fabricated via the thermal non-solvent induced phase separation method exhibited remarkable organic dye retention and oil absorption capabilities. Specifically, the methylene blue retention rate increased by 40.7%, and

the oil absorption capacity enhanced by 54.9%. Shen *et al.* [16] investigated the electrospinning of three branched PLA porous materials. They discovered that these microspheres had a higher tendency to adsorb positively charged drugs in an aqueous solution. By manipulating solvents with different dielectric constants, they could control the size of the microspheres. Moreover, SEM observations revealed that as the number of pores increased, more silver ions were adsorbed [17-21].

The PLA is a hydrophobic material with decent mechanical properties. However, its toughness is a limiting factor. In contrast, GO, featuring an abundance of functional groups, is more reactive than graphite [22-26]. The presence of numerous hydroxyl and carbonyl groups imparts good hydrophilicity to GO. Additionally, its layered structure provides a large specific surface area, and it exhibits excellent mechanical properties [27-31]. Thus, combining PLA and GO to create composite nanomaterials allows for the full exploitation of the unique advantages of both materials.

As illustrated in fig. 1, in this research, we harnessed the spiral electrospinning technology to fabricate nanofiber membranes [32-35]. Initially, a series of orthogonal experiments were meticulously designed and executed to identify the optimal process parameters for preparing pure PLA porous nanofibers. This step was crucial as it laid the foundation for subsequent experiments with the composite material.

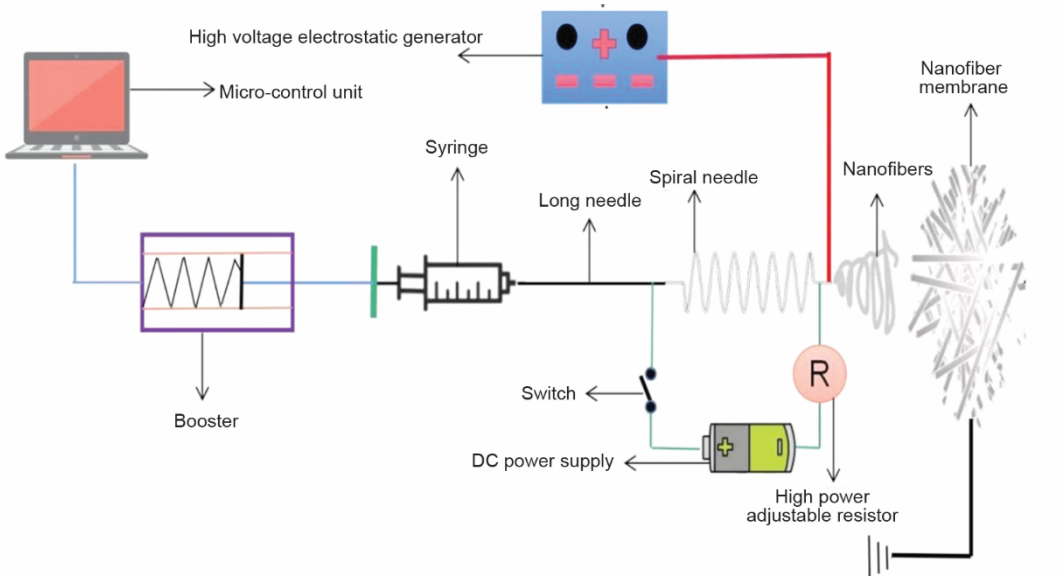


**Figure 1. Schematic diagram of spiral electrospinning (needle helix number is 9)**

Subsequently, we combined PLA and GO, two environmentally friendly and non-polluting materials, to synthesize PLA/GO porous nanofibers. The integration of these materials was expected to leverage their respective advantages and endow the composite nanofibers with unique properties.

To comprehensively understand the characteristics of these nanofibers, we employed a suite of advanced analytical techniques. Fourier transform infrared spectroscopy (FTIR) was used to analyze the chemical functional groups present in the nanofibers, providing insights into their molecular structure. The X-ray diffraction (XRD) was applied to study the crystallinity and phase composition of the materials, which is vital for understanding their physical

properties. Pore structure analysis was carried out to determine the pore size distribution, porosity, and specific surface area of the nanofibers, all of which are key factors influencing their adsorption performance. Mechanical testing was performed to evaluate the mechanical strength and flexibility of the nanofibers, essential for practical applications. Contact angle measurements were conducted to assess the wettability of the nanofiber membranes, which is closely related to their surface properties.

By exploring the inherent characteristics of PLA/GO porous nanofibers through these comprehensive characterizations, we aimed to establish a fundamental understanding of their structure property relationships. This knowledge is of paramount significance as it can serve as a guide for future research on the adsorption performance of PLA/GO porous nanofibers, potentially opening up new avenues for applications in various fields such as environmental remediation, drug delivery, and tissue engineering.

## Experimental materials and reagents

All materials and chemical reagents employed in this study were of analytical grade and used without further purification. The PLA, with a molecular weight of 100000, denoted as $M_w$ = 100000, was sourced from Shenzhen Guanghua Weiye Co., Ltd. The GO was procured from Suzhou Gree Pharmaceutical Technology Co., Ltd. Deionized water – DW (Inspire s200) was supplied by Shanghai Yudong Water Treatment Co., Ltd. N-N-dimethylformamide (DMF, $M_w$ = 73.09) and dichloromethane (DCM, $M_w$ = 84.93) were obtained from Shanghai Chemical Reagent Co., Ltd. These carefully selected and unpurified materials served as the foundation for the preparation of the experimental samples, ensuring the reliability and reproducibility of the subsequent experimental results.

## Experimental instruments and equipment

The experimental set-up relied on a carefully selected array of instruments and equipment, each sourced from reputable manufacturers to ensure precision and reliability.

A constant flow injection pump (ISP01 - A), supplied by Baoding Lange Constant Flow Pump Co., Ltd., was utilized to precisely regulate the flow rate of the spinning solution, a crucial factor in the electrospinning process. The high voltage electrostatic generator (DW - P403 - 1ACCC), provided by Dongwen High Voltage Power Supply Co., Ltd., generated the necessary electrostatic field for electrospinning, facilitating the formation of nanofibers.

An ultrasonic cleaning machine (SL - 5200DT) from Nanjing Shunliu Instrument Co., Ltd. was employed for thorough cleaning of equipment and glassware, as well as for promoting the dispersion of materials during sample preparation. The electronic balance (CP214), manufactured by Ohaus Instruments Co., Ltd., enabled accurate weighing of substances, ensuring the precise formulation of solutions.

The electric constant temperature drying oven (DHG - 924A), provided by Shanghai Pudong Rongfeng Scientific Instrument Co., Ltd., was used to dry samples at a controlled temperature, eliminating residual solvents and stabilizing the samples for subsequent analysis. A magnetic stirrer (HJ - 6A) from Gongyi Yuhua Instrument Co., Ltd. facilitated homogeneous mixing of solutions, ensuring uniform distribution of components.

For structural analysis, an XRD (Philips XPert - Pro MPD) by PANalytical (The Kingdom of the Netherlands) was utilized to determine the crystal structure of the samples. The universal material testing machine (INSTRON - 3365), supplied by INSTRON (America), was employed to evaluate the mechanical properties of the nanofiber membranes, measuring parameters such as breaking strength and elongation at break.

The fully automatic specific surface porosity tester (POROMETER 3G) from Quantachrome Instruments (America) was used to analyze the pore structure of the samples, providing valuable insights into pore size distribution, porosity, and specific surface area. The contact angle (Kruss DSA 100) Tester, provided by TA Instrument (America), measured the wetting properties of the nanofiber membranes, determining their surface hydrophilicity or hydrophobicity. A FTIR from Nicolet (America) was employed to identify chemical functional groups present in the samples, aiding in the characterization of their chemical composition.

In addition to these major instruments, a variety of auxiliary items were also integral to the experiment. These included 30 mL and 50 mL brown reagent bottles for storing solutions, protecting them from light induced reactions. Disposable sterilized syringes (10 mL) were used for accurate transfer and dispensing of solutions. Weighing paper, aluminum foil, sealing glue, and self sealing bags were essential for sample handling, storage, and protection, maintaining the integrity of the samples throughout the experimental process.

### Preparation of PLA/GO solution

Based on the optimized process parameters for the solute and solvent of pure PLA, varying proportions of GO, specifically 0.1 wt.%, 0.2 wt.%, 0.5 wt.%, and 1.0 wt.%, were incorporated into N,N-dimethylformamide (DMF). The GO-DMF mixtures were then subjected to 2 hours ultrasonic oscillation. This ultrasonic treatment was crucial for achieving a homogeneous dispersion of GO in DMF, breaking down any potential aggregates and ensuring a uniform distribution at the nanoscale.

Subsequently, 8 wt.% of PLA and dichloromethane (DCM) were added to the dispersed GO-DMF solutions. The solvent ratio was precisely maintained at DCM:DMF = 9:1, a ratio carefully determined to optimize the electrospinning process and the formation of the desired nanofiber morphology. After the addition of all components, the mixtures were stirred at room temperature for 6 hours. This extended stirring period facilitated thorough mixing of the polymers and solvents, promoting the formation of a stable and homogeneous solution.

Prior to the electrospinning process, the solutions were sonicated for an additional 30 minutes. This final sonication step further enhanced the dispersion of the components, ensuring that any remaining agglomerates were disrupted and that the solution was in an optimal state for electrospinning.

The prepared spinning solutions were transferred to brown wide mouth bottles. The use of brown bottles was essential as it effectively shielded DCM from light, preventing potential photocatalysis. The DCM is sensitive to light, and photocatalysis could lead to chemical changes in the solution, affecting the properties of the resulting nanofibers. Moreover, strict attention was paid to the sealing of these brown wide mouth bottles. This was to prevent the volatilization of DCM, which could alter the composition of the spinning solution and ultimately impact the quality and reproducibility of the electrospun nanofibers.

### The PLA/GO porous nanofiber spinning

Ten milliliters of the prepared spinning solution were carefully drawn into a disposable syringe. Subsequently, any internal air was meticulously expelled to ensure a consistent flow of the solution. The syringe was then securely fixed onto a constant flow injection pump.

Drawing on the optimized parameters established for pure PLA, a spinning voltage of 20 kV and a spinning distance of 18 cm were selected. These values were determined to be conducive to the formation of high quality nanofibers with the desired morphology. Simulta-

neously, a 20 cm × 20 cm aluminum foil paper was set as the receiving plate, providing a large surface area and conductive medium for the deposition of nanofibers.

The spinning speed was precisely set at 1 mL per hour. This rate was optimized to balance the production of nanofibers and their uniform deposition on the receiving plate. The ambient temperature was maintained at 25 ±1 °C, and the humidity was regulated to 55 ±1 %. These environmental conditions were carefully controlled as they significantly influenced the evaporation rate of the solvents in the spinning solution, which in turn affected the nanofiber formation process.

To prevent DCM in the spinning solution from undergoing photocatalysis during the spinning process, appropriate shading measures were implemented. Photocatalysis of DCM could lead to chemical changes in the solution, potentially altering the properties of the resulting nanofibers. By controlling these parameters and environmental conditions, the electrospinning process was optimized to fabricate PLA/GO porous nanofibers with consistent and reproducible characteristics.

**Performance characterization**

The porous nanofiber membranes with varying GO contents underwent a meticulous pre-treatment process. Initially, they were dried at room temperature for 24 hours to remove any residual solvents or moisture. This step was crucial as it ensured the stability and integrity of the samples for subsequent analysis. After drying, the membranes were carefully cut into powder form and placed in a 15 mm × 15 mm sample holder, which was then used for XRD analysis.

The XRD measurements of the fiber membranes were carried out using an X-ray diffractometer. A Cu target served as the radiation source, operating at a tube voltage of 40 kV and a tube current of 40 mA. The diffraction angle range was set from 5° to 50°, and the scanning speed was maintained at 2° per minute. These parameters were carefully selected to obtain high quality diffraction patterns that could accurately reveal the crystal structure of the nanofibers and provide insights into the interaction between PLA and GO within the composite membranes.

To explore the impact of different GO contents on the pore structure of PLA fiber membranes, a pore size distribution analysis was conducted using an automated specific surface area and pore size analyzer. The fiber membranes were prepared into circular samples with a diameter of 25 mm, approximately the size of a coin. This standard size was chosen to ensure consistent and accurate measurements. The samples were then fully wetted with porofil solution in a glass dish. This wetting process was essential as it allowed for the proper filling of the pores, enabling accurate determination of the pore size distribution. After wetting, the samples were carefully placed flat in the testing instrument. The pore size distribution of the fiber membrane samples was measured in both wet and dry states to comprehensively understand the pore characteristics. Each fiber membrane was used only once for measurement to avoid any errors or artifacts caused by repeated use. By continuously replacing the samples, the initially set pore size range was optimized to obtain a standard S-shaped measurement curve, which is a reliable indicator for accurate pore size determination. All relevant data were meticulously recorded for further analysis.

The mechanical properties, specifically the breaking strength and elongation at break, of the fiber membranes were determined using a universal material testing machine. First, rectangular samples with dimensions of 40 mm × 10 mm were carefully prepared from the nanofiber membranes. To ensure consistent and accurate testing, the ends of the samples

were wrapped with aluminum foil, leaving a 10 mm × 10 mm section exposed for the stretching test. The thickness of the fiber membrane was measured at three different positions using a screw micrometer, and the average value was calculated. This average thickness was used to accurately calculate the mechanical properties. Before the stretching test, the samples were placed in a constant temperature and humidity chamber for 24 hours to equilibrate them to a standard environment. This step was necessary to minimize the influence of environmental factors on the mechanical properties. The stretching test was then performed on the section of the sample with uniform thickness. The test distance was set at 20 mm, and the stretching speed was 20 mm per minute. Each sample was measured 5 times, and the average value was calculated to improve the reliability and accuracy of the results. The obtained data were carefully organized, and the breaking strength and elongation at break of the fiber membrane were calculated using specific formulas, eqs. (1) and (2), providing quantitative information about the mechanical performance of the nanofiber membranes.

$$\text{Breaking strength [MPa]} = \frac{\text{Breaking power [N]}}{\text{Thicknesses [mm]} \times \text{Height [mm]}} \tag{1}$$

$$\text{Elongation at break [\%]} = \frac{\text{Fiber membrane elongation [mm]}}{\text{Fiber membrane original length [mm]}} 100\% \tag{2}$$

The wetting performance of the fiber membranes under test was evaluated by measuring their contact angles in static conditions using a contact angle instrument. The DW was drawn into a syringe, with each drop having a volume of approximately 6 μL. To obtain a reliable average contact angle value, each sample was tested at five different positions. During the measurement process, the smooth edge region of the fiber membrane was carefully selected. This was to ensure that the measurement results were as accurate as possible, as irregular or rough areas could introduce errors in the contact angle determination.

Following the preparation of the porous nanofiber membranes with varying GO contents, they were air dried at a constant temperature within a fume hood for 24 hours. This drying step was crucial for removing any remaining solvents or moisture. After drying, the membranes were carefully detached from the aluminum foil substrate and then analyzed using an intelligent FTIR spectrometer (NICOLET 5700). The scanning process was carried out 16 times to enhance the signal-to-noise ratio and improve the accuracy of the spectral data. The scanning range was set from 500 $cm^{-1}$ to 4000 $cm^{-1}$, with a resolution of 4 $cm^{-1}$.

## Results and analysis

As depicted in fig. 2(a), the FTIR spectrum of GO exhibits distinct features. Specifically, symmetrical stretching peaks of the C-O-C bond are clearly visible at 1092 $cm^{-1}$ and 1400 $cm^{-1}$. Additionally, stretching vibration peaks of H-O and C=C bonds are observed at 1620 $cm^{-1}$, stretching vibration peaks of the C=O bond at 1746 $cm^{-1}$, and stretching vibration peaks of the O-H bond at 3394 $cm^{-1}$. In fig. 2(b), which shows the FTIR spectra of PLA/GO fibers with different GO contents, curve An represents the spectrum of pure PLA. The PLA also has characteristic C-O-C bond peaks at 1092 $cm^{-1}$ and 1400 $cm^{-1}$, along with a stretching peak at 1753 $cm^{-1}$, a vibration peak at 2940 $cm^{-1}$, and an O-H vibration peak at 3508 $cm^{-1}$. Given the relatively simple molecular structure of PLA, where the relevant functional groups are located at the molecular chain ends, the stretching vibration peaks appear relatively gentle.

Notably, due to the similarities in the infrared spectra of GO and PLA, it is challenging to definitively conclude whether GO has been successfully incorporated into the porous PLA nanofibers based solely on these FTIR results. Therefore, additional experimental tests and more in-depth characterizations are necessary to accurately determine the incorporation and distribution of GO within the PLA nanofiber matrix.

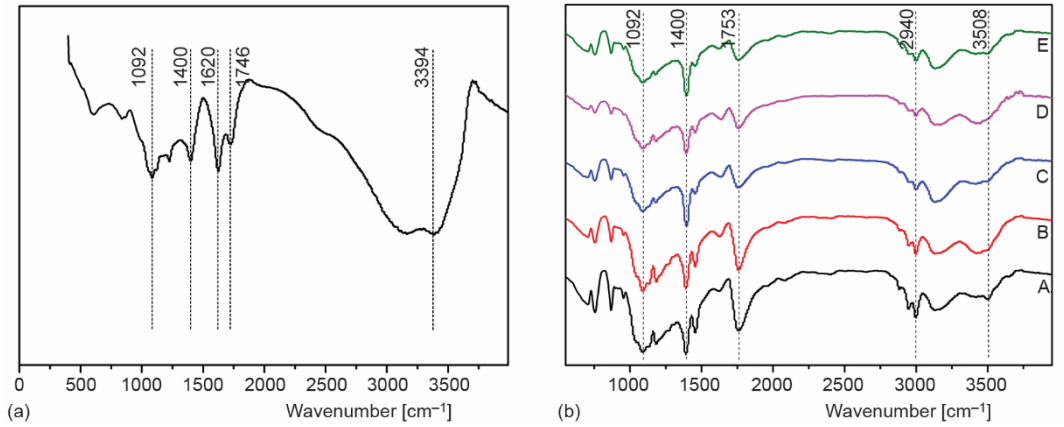


**Figure 2. (a) The FTIR of GO and (b) FTIR of PLA/GO nanofibers with different go contents (A – pure PLA, B – 0.1 wt.% GO, C – 0.2 wt.% GO, D – 0.5 wt.% GO, E – 1.0 wt.% GO)**

Figure 3(a) presents the XRD pattern of pure PLA, while fig. 3(b) displays the XRD patterns of PLA/GO fibers with varying GO contents. In fig. 3(a), a pronounced reflection is detected at $2\theta = 17°$, which corresponds to the characteristic peak of PLA. The XRD analysis reveals that the peak of the PLA XRD curve lacks the sharpness of the GO peak, instead manifesting as a *bread-like* peak. This morphological feature indicates that PLA is a semi-crystalline polymer, characterized by its coexistence of ordered crystalline regions and disordered amorphous regions.

In fig. 3(b), a distinct diffraction peak emerges at $2\theta = 10°$, which can be attributed to GO. As the content of GO increases, the intensity of this peak becomes more pronounced. Notably, in curves C and D, corresponding to higher GO loadings, the GO peak exhibits remarkable sharpness, reaching its maximum intensity when the GO content is 1.0 wt.%. The peak position of GO is subject to shifts due to variations in the interaction with water molecules. Consequently, at lower GO contents of 0.1 wt.% and 0.2 wt.%, the $2\theta$ values are slightly greater than 10°, likely due to the influence of water related interactions on the diffraction characteristics of GO.

Overall, the XRD results clearly demonstrate that GO is effectively incorporated into the interior of the fibers. Moreover, the addition of GO does not give rise to any new crystal structures within the porous PLA/GO nanofibers. Both GO and PLA retain their original crystal structures, suggesting that the composite formation process does not induce significant structural transformations in either component at the crystalline level. This finding provides valuable insights into the compatibility and structural integrity of the PLA/GO nanofiber composites, laying a foundation for further exploration of their functional properties and potential applications.

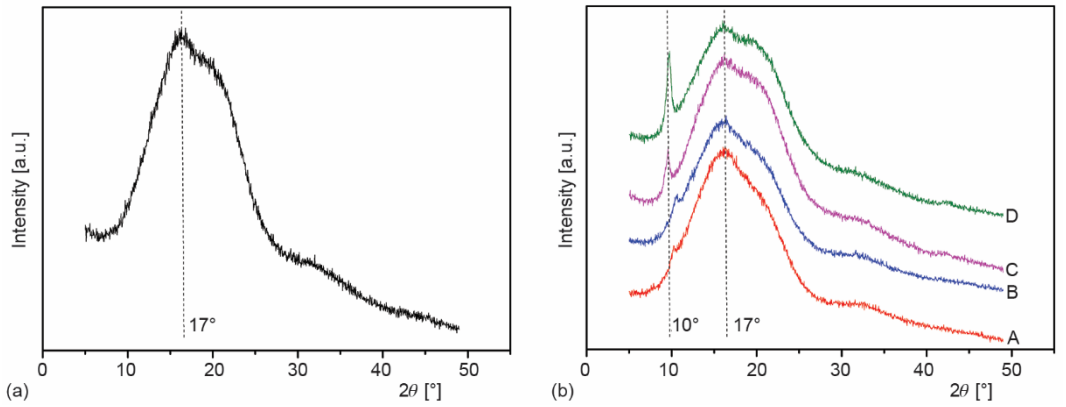


**Figure 3. (a) The XRD of pure PLA nanofibers and (b) XRD of PLA/GO nanofibers with different go content (A – 0.1 wt.% GO, B – 0.2 wt.% GO, C – 0.5 wt.% GO, D – 1.0 wt.% GO)**

Figure 4 illustrates the pore size distributions of pure PLA porous nanofibers and PLA/GO porous nanofibers with different GO contents. In fig. 4(a), representing pure PLA nanofibers, the pore size of 8.106 μm constitutes the largest proportion of the total pores, accounting for 8.12%. Upon adding 0.1 wt.% of GO, the pore size with the highest proportion of total pores drops sharply to 4.151 μm, which accounts for 11.08% of the total pores. When the GO content is increased to 0.2 wt.%, the overall trend of the total pore size distribution remains similar to that at 0.1 wt.% GO. At a GO content of 0.5 wt.%, the pore size of 3.387 μm represents the largest proportion of total pores, reaching 16.41%. Similar to the patterns in figs. 4(a)-4(c), the distribution curves exhibit two peaks, with the smaller peak positioned to the right of the larger one, indicating the presence of smaller sized pores. When the GO content reaches 1.0 wt.%, the pore size distribution becomes the most concentrated, with a dominant pore size of 3.161 μm, accounting for 20.71% of the total pores.

Table 1 presents the pore related data for pure PLA porous nanofibers and PLA/GO nanofibers with varying GO contents. Analysis of tab. 1 reveals that as the GO content increases, the total number of pores in the fibers steadily rises. Specifically, at a GO content of 0.5 wt.%, the total number of pores is 11.5 times that of pure PLA. Conversely, the average pore size decreases. In fact, the average pore size of pure PLA is 2.5 times that of the nanofibers with 0.5 wt.% GO. The incorporation of GO into PLA nanofibers effectively transforms large pores into smaller ones, significantly increasing the total pore count and making the pore size distribution more concentrated, thereby enhancing the pore density.

**Table 1. Pore size data of pure PLA porous nanofibers and PLA/GO nanofibers with different go contents**

| Serial number | GO concentration [wt.%] | Aperture size [μm] | Average aperture size [μm] | Pore density [per $cm^{-2}$] | Total number of pores [tonne $cm^{-2}$] |
|---|---|---|---|---|---|
| 1 | 0 | 6.74~10.1 | 8.42 | $2.023\times10^{5}$ | $2.231\times10^{6}$ |
| 2 | 0.1 | 3.18~5.6 | 4.09 | $1.918\times10^{6}$ | $1.731\times10^{7}$ |
| 3 | 0.2 | 3.05~5.66 | 3.96 | $1.806\times10^{6}$ | $1.742\times10^{7}$ |
| 4 | 0.5 | 2.73~4.1 | 3.33 | $4.202\times10^{6}$ | $2.562\times10^{7}$ |
| 5 | 1.0 | 2.56~3.84 | 3.00 | $4.414\times10^{6}$ | $2.131\times10^{7}$ |

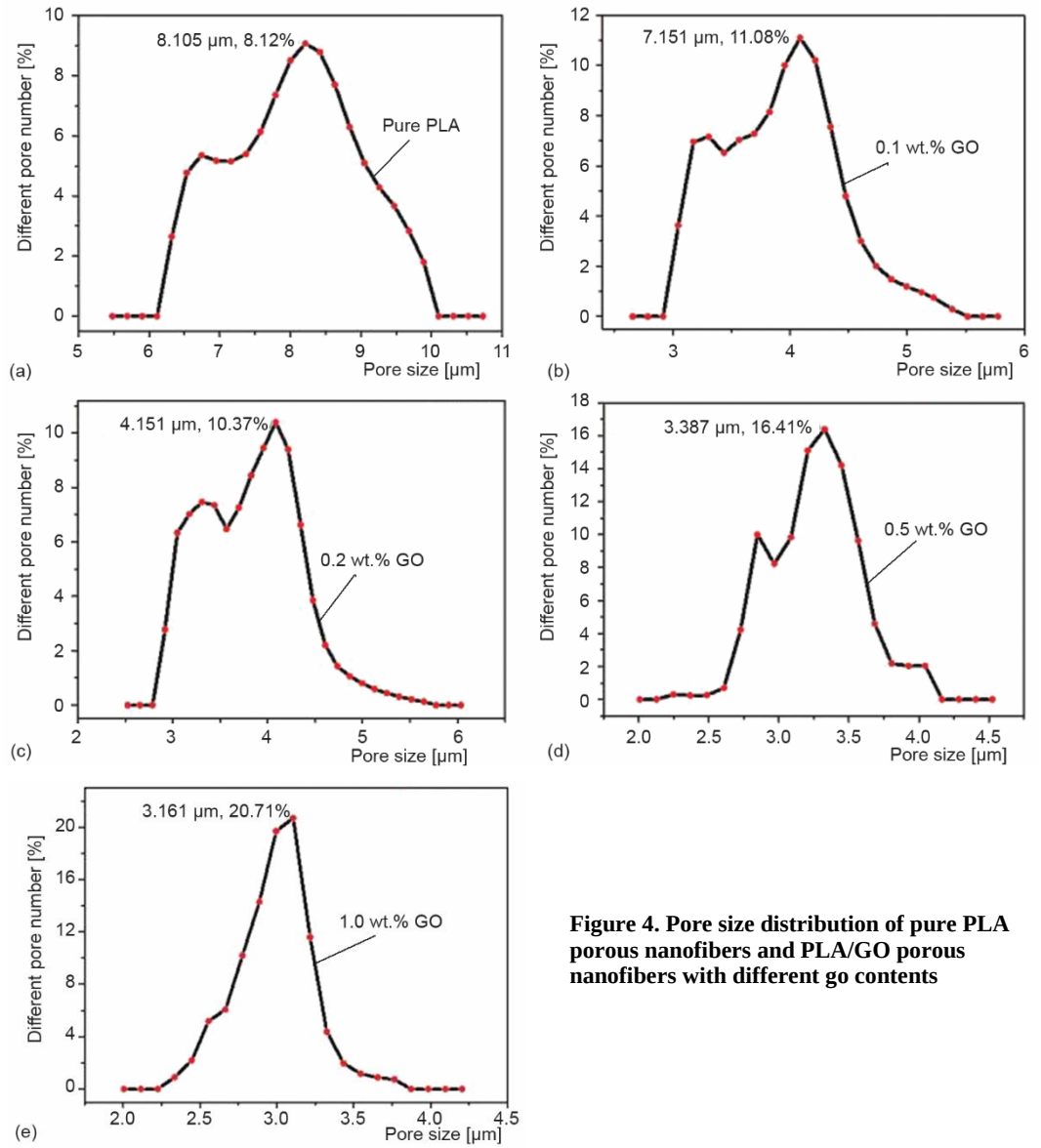


**Figure 4. Pore size distribution of pure PLA porous nanofibers and PLA/GO porous nanofibers with different go contents**

The mechanical properties, namely the breaking strength and elongation at break, of the fiber membranes are depicted in fig. 5. Notably, the breaking strength of pure PLA is markedly lower than that of the PLA/GO porous nanofibers. As the GO content increases, the breaking strength of the fiber membranes initially improves. At a GO content of 0.5 wt.%, the fiber breaking strength reaches a peak of 1.98 MPa. However, with a further increase in GO content, GO tends to agglomerate between fibers, which slightly diminishes the breaking strength. Given that PLA inherently possesses a degree of brittleness, the elongation at break of the pure PLA fiber membrane is 74.7%. When the GO content is increased by just 0.1 wt.%, there is no substantial change in the fiber elongation at break. Yet, as the GO con-

tent continues to rise, the elongation at break increases significantly. Specifically, at a GO content of 0.5 wt.%, the elongation at break of the PLA fiber increases by 25% compared to pure PLA fibers. When the GO content reaches 1.0 wt.%, this value increases by 31% relative to pure PLA fibers. These results clearly demonstrate that the addition of GO effectively optimizes both the breaking strength and elongation at break of the PLA/GO porous nanofibers.

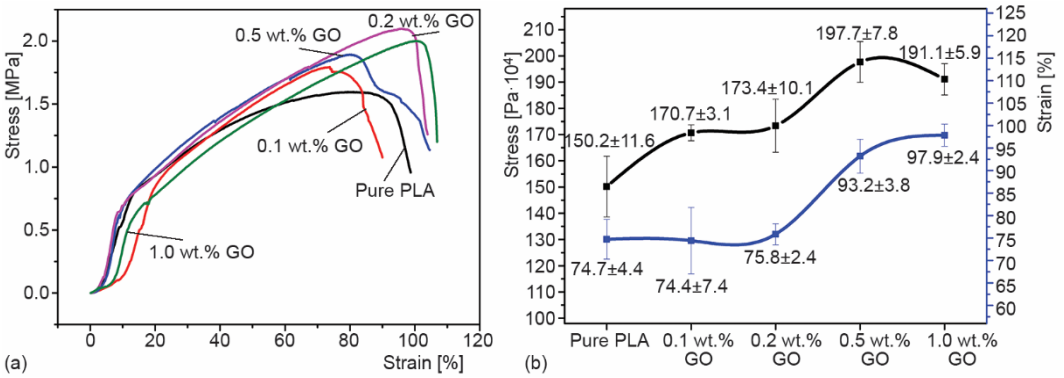


**Figure 5. Mechanical property tests of pure PLA porous nanofibers and PLA/GO porous nanofibers with different go contents**

Figure 6 displays the contact angle data and visual images of pure PLA fibers and PLA/GO fibers (membranes) with varying GO contents. As depicted in fig. 6, the contact angle of pure PLA fibers measures 157.4 ±10.0°, signifying superhydrophobic behavior. In contrast, GO is a hydrophilic material that has the ability to dissolve in water. Nevertheless, within the spinning solvent, the proportion of GO is notably lower than that of PLA, rendering it challenging to alter the hydrophobic nature of the composite fibers. When the GO content is 0.5 wt.%, the contact angle decreases to 146.5 ± 5.05°, representing a reduction of 10.9°. Even when the GO content reaches 1.0 wt.%, GO has a tendency to agglomerate between the fibers, making it difficult to achieve uniform distribution. As a result, the contact angle of the fibers does not experience a significant decrease.

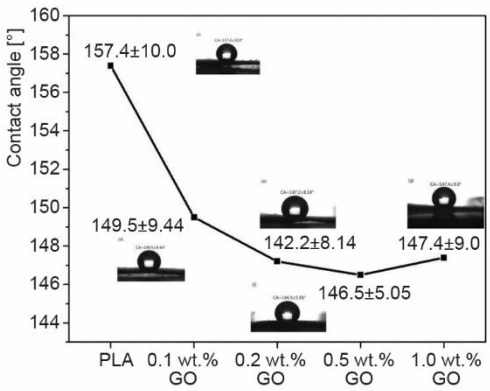


**Figure 6. Contact angle data of PLA and PLA/GO fibers with different go contents**

## Conclusion

In comparison to pure PLA fibers, PLA/GO porous nanofibers showcase remarkably enhanced mechanical properties. Both the fiber breaking strength and elongation at break are significantly elevated. The incorporation of GO has a negligible impact on the crystal structures within the porous PLA/GO nanofibers. As the content of oxidized graphite increases, the average pore size decreases and the total number of pores increases. Similarly, it does not substantially influence the wetting properties of the fiber membranes. Consequently, PLA/GO

porous nanofibers are capable of maintaining their inherent adsorption performance while achieving significant improvements in their mechanical properties. This provides a solid foundation for further in-depth research into the adsorption properties of PLA/GO porous nanofibers, opening up potential applications in various fields such as environmental remediation, drug delivery systems, and filtration technologies.

## Acknowledgment

Jianming Wang and Ya Chen are co-first authors of this article. This work is supported by National Foreign Experts Program of the Ministry of Education (G2023014001L). The work is also funded by Qing Lan Project of Jiangsu Colleges and Universities for Excellent Teaching Team in 2023, Letter from the Faculty Department of Jiangsu Provincial Department of Education (2023) No. 27, the doctoral research initiation fund project of Yancheng Polytechnic College (2023), Jiangsu Province Higher Vocational Education High-level Major Group Construction Project-Modern Textile Technology Major Group (Grant number: Jiangsu Vocational Education 2020. No 31). Yancheng Polytechnic College Science and Technology Innovation Team Funding Project, [2025] No. 6, also supports the research of this subject. Key technology innovation platform for flame retardant fiber and functional textiles in Jiangsu Province (2022JMRH-003) also supports this research.

## References

[1] He, C.-H., *et al.*, A Fractal Model for the Internal Temperature Response of a Porous Concrete, *Applied and Computational Mathematics*, *21* (2022), 1, pp. 71-77
[2] He, C.-H., Liu, C., Fractal Dimensions of a Porous Concrete and Its Effect on the Concrete's Strength. *Facta Universitatis - Series Mechanical Engineering*, *21* (2023), 1, pp. 137-150
[3] Jin, X. H., *et al.*, Influencing Factors of Deformation and Failure of Porous Coal Under Conventional Loading, *Facta Universitatis - Series Mechanical Engineering*, *23* (2025), 1, pp. 161-170
[4] Zheng, J. Y., Wang, L. K., Experimental Study on Creep Loading of Porous Coal Under Different Influencing Factors, *Facta Universitatis - Series Mechanical Engineering*, *22* (2024), 1, pp. 153-163
[5] Li, X. X., *et al.*, Elucidating the Fractal Nature of the Porosity of Nanofiber Members in the Electrospinning Process, *Fractals*, *32* (2024), 2450109
[6] Du, Y., *et al.* Covalent Functionalization of Graphene Oxide with Porphyrin and Porphyrin Incorporated Polymers for Optical Limiting, *Physical Chemistry Chemical Physics*, *19* (2017), 3, pp. 2252-2260
[7] Wang, J., Chen, H., Catalytic Ozonation for Water and Wastewater Treatment: Recent Advances and Perspective, *Science of the Total Environment*, *704* (2019), 135249
[8] Chen, Y., *et al.*, Mechanics of Emulsion Electrospun Porous Carbon Fibers as Building Blocks of Multifunctional Materials, *ACS Applied Materials & Interfaces*, *10* (2018), 44
[9] Xue J, *et al.*, Electrospun Nanofibers: New Concepts, Materials, and Applications, *Accounts of Chemical Research*, *50* (2017), 8, pp. 1976-1987
[10] Bognitzki, M., *et al.*, Nanostructured Fibers via Electrospinning, *Advanced Materials*, *13* (2001), 1, pp. 70-72
[11] Zhu, J., *et al.*, Electrospinning Poly (L-Lactic Acid) Piezoelectric Ordered Porous Nanofibers for Strain Sensing and Energy Harvesting, *Journal of Materials Science: Materials in Electronics*, *28* (2017), 16, pp. 12080-12085
[12] Li, S., *et al.* Fabrication of Unique Ribbon-Like Porous $LaFeO_3$ Nanofibers Photocatalyst via Electrospinning, *Applied Physics A*, *117* (2014), 3, pp. 1381-1386
[13] Chen, Z., *et al.*, Preparation of Aminated Polyacrylonitrile Porous Fiber Mat and Its Application for Cr (VI) Ion Removal, *Fibers and Polymers*, *15* (2014), 7, pp. 1364-1368
[14] Lyoo. W. S., *et al.*, Preparation of Porous Ultra-Fine Poly (Vinyl Cinnamate) Fibers, *Materials Letters*, *59* (2005), 28, pp. 3558-3562
[15] Li, X., *et al.*, Electrospun Preparation of Polylactic Acid Nanoporous Fiber Membranes via Thermal-Nonsolvent Induced Phase Separation, *Journal of the Taiwan Institute of Chemical Engineers*, *60* (2016), Mar., pp. 636-642

[16] Shen, W., *et al.*, Research on Electrospinning Three-Branched-Chain PLA Porous Microspheres and Adsorption for Silver Ions, *Journal of Applied Polymer Science*, *135* (2018), 46735
[17] Li, X. X., He, J.-H., Bubble Electrospinning with an Auxiliary Electrode and an Auxiliary Air Flow, *Recent Patents on Nanotechnology*, *14* (2020), 1, pp. 42-45
[18] He, J.-H., *et al.* The Maximal Wrinkle Angle During the Bubble Collapse and Its Application to the Bubble Electrospinning, *Frontiers in Materials*, *8* (2022), 800567
[19] Qian, M. Y. He, J.-H. Collection of Polymer Bubble as a Nanoscale Membrane, *Surfaces and Interface*, *28* (2022), 101665
[20] Tian, D., He, J.-H., Macromolecular Electrospinning: Basic Concept & Preliminary Experiment, *Results in Physics*, *11* (2018), Dec., pp. 740-742
[21] Tian, D., *et al.*, Macromolecule Orientation in Nanofibers, *Nanomaterials*, *8* (2018), 918
[22] Tian, D., He, J.-H., Self-Assemble of Macromolecules in a Long and Narrow Tube, *Thermal Science*, *22* (2018), 4, pp. 1659-1664
[23] Tian, D., He, J.-H., Macromolecular-Scale Electrospinning: Controlling Inner Topologic Structure Through a Blowing Air, *Thermal Science*, *26* (2022), 3B, pp. 2663-2666
[24] Li, X. X., *et al.*, Boosting Piezoelectric and Triboelectric Effects of PVDF Nanofiber through Carbon-Coated Piezoelectric Nanoparticles for Highly Sensitive Wearable Sensors, *Chemical Engineering Journal*, *426* (2021), 130345
[25] Peng, N. B., He, J.-H., Insight into the Wetting Property of a Nanofiber Membrane by the Geometrical Potential, *Recent Patents on Nanotechnology*, *14* (2020), 1, pp. 64-70
[26] Li, X. X., *et al.*, High Energy Surface as a Receptor in Electrospinning: A Good Switch for Hydrophobicity to Hydrophilicity, *Thermal Science*, *25* (2021), 3B, pp. 2205-2212
[27] He, J.-H., Elazem, N. Y. A., The Carbon Nanotube-Embedded Boundary Layer Theory for Energy Harvesting, *Facta Universitatis Series: Mechanical Engineering*, *20* (2022), 2, pp. 211-235
[28] Kou, S. J., *et al.*, Fractal Boundary Layer and its Basic Properties, *Fractals*, *30* (2023), 2250172
[29] Kumar, K., *et al.*, Irreversibility Analysis in $Al_2O_3$-Water Nanofluid Flow with Variable Property, *Facta Universitatis Series: Mechanical Engineering*, *20* (2022), 3, pp. 503-518
[30] He, C.-H., A Variational Principle for a Fractal Nano/Microelectromechanical (N/MEMS) System, *International Journal of Numerical Methods for Heat & Fluid Flow*, *33* (2023), 1, pp. 351-359
[31] He, J.-H., *et al.*, Pull-in Stability of a Fractal MEMS System and its Pull-in Plateau, *Fractals*, *30* (2022), 2250185
[32] Zhao, L., Preparation and Properties of PVA Nanofibers with Spiral Ordered Internal Structure, *Materials Research Express*, *10* (2023), 065006
[33] Zhao, L., *et al.*, Preparation and Properties of PAN Nanofiber Membrane Based on Spiral Spinning Technology, *Journal of Engineered Fibers and Fabrics*, *2023* (2023), 18
[34] Wei, L., *et al.*, Preparation and Adsorption Application of PLA/GO/PDA Nanofiber Membrane, *Materials Research Express*, *11* (2024), 115006
[35] Zhao, L., *et al.*, A Spider-Inspired Electrospinning for Fabrication of PVDF Nanofiber Membranes, *Thermal Science*, *28* (2024), 3A, pp. 2251-2258

Paper submitted: October 10, 2024
Paper revised: May 15, 2025
Paper accepted: May 23, 2025